ACS OMEGA

Open Access

http://pubs.acs.org/journal/acsodf

Article

Structure Elucidation and Interaction Dynamics of MefA-MsrD Efflux Proteins in *Streptococcus pneumoniae*: Impact on Macrolide Susceptibility

Sreeram Chandra Murthy Peela, Soumya Basu, Jyoti Sharma, Abdullah F. AlAsmari, Fawaz AlAsmari, Sultan Alalmaee, Sudha Ramaiah, Sujatha Sistla,* Paul Livingstone,* and Anand Anbarasu*

Cite This: *ACS Omega* 2023, 8, 39454−39467

Read Online

ACCESS | Metrics & More | Article Recommendations | Supporting Information

ABSTRACT: Macrolides are empirically used to treat bacterial community-acquired pneumonia (CAP). *Streptococcus pneumoniae*, being the major pathogen responsible for bacterial CAP with high mortality rates, express MefA-MsrD efflux pumps to hinder macrolide susceptibility. Despite its importance, the structural features of the efflux-protein complex and its impact on macrolide susceptibility have not yet been elucidated explicitly. Therefore, in the present study, combining homology, threading, and dynamics approaches, MefA and MsrD proteins in pathogenic *S. pneumoniae* were modeled. Both membrane (lipid-bilayer) and cytoplasmic (aqueous) environments were considered to simulate the MefA and MsrD proteins in their ideal cellular conditions followed by dynamics analyses. The simulated MefA structure represented a typical major facilitator superfamily protein structure with 13 transmembrane helices. MefA-MsrD interaction via clustering-based docking revealed low-energy conformers with stable intermolecular interactions. The higher clinical MIC value of azithromycin over erythromycin was reflected upon erythromycin eliciting stronger interactions (dissociation constant or k_i = ∼52 μM) with the cytoplasmic ATP-binding MsrD than azithromycin (k_i = ∼112 μM). The strong (binding energy = −132.1 ± 9.5 kcal/mol) and highly stable (root-mean-square fluctuation < 1.0 Å) physical association between MefA with MsrD was validated and was found to be unaffected by the antibiotic binding. Higher propensity of the macrolides to interact with MsrD than MefA established the importance of the former in macrolide susceptibility. Ours is probably the first report on the structural arrangements in the MefA-MsrD efflux complex and the macrolide susceptibility in *S. pneumoniae*. This study provides a novel lead for experimental explorations and efflux-pump inhibitor designs.

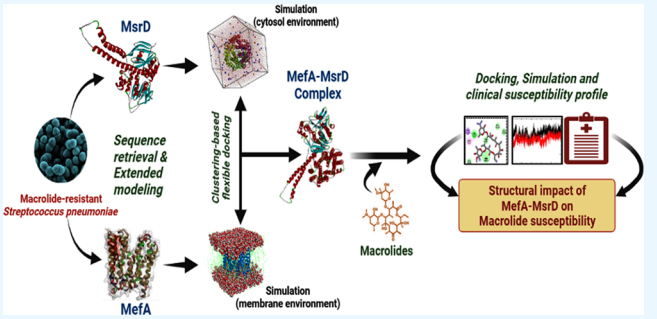

1. INTRODUCTION

Macrolides are one of the commonly prescribed antibiotics for treating respiratory infections. They act by inhibiting bacterial protein synthesis and are bacteriostatic or bactericidal depending on their concentration and the bacteria. While it continues to be given as empirical therapy, there is a substantial rise of resistance to this group of antibiotics globally in pathogens like *Streptococcus pneumoniae* that cause lower respiratory tract infections. *S. pneumoniae,* as the causative agent of acute bacterial meningitis, pneumonia, and febrile bacteremia, has threatened the global population especially the children and elderly with high mortality.[1] Recent reports further highlighted the increased mortality due to invasive pneumococcal infections post COVID-19 infections in various parts of the world.[2,3] Although multiple targets, especially the different penicillin-binding proteins in *S. pneumoniae*, have widely been exploited for therapeutic intervention for decades, the rise of penicillin resistance post 2000 has raised major concerns worldwide.[4] The desensitization to penicillin is another major reason for use of alternative antibiotics such as macrolides.[5] The use of macrolides was also challenged by resistance to macrolides [in 35.1% of the community-acquired pneumonia (CAP) patients] in *S. pneumoniae*. Two mechanisms contributed to the macrolide resistance, viz., efflux-mediated (encoded by MefA) and ribosomal methylation (mediated by ErmB).[6] There are less common mechanisms like mutations in 23S-rRNA regions like L4 and domain V as well.[7]

In a previous study from our group, efflux-mediated macrolide resistance was detected in majority of the macrolide-resistant isolates.[6] This invoked us to delve deeper into the macrolide efflux protein of pneumococci, and we observed that

Received: July 19, 2023
Accepted: September 28, 2023
Published: October 10, 2023

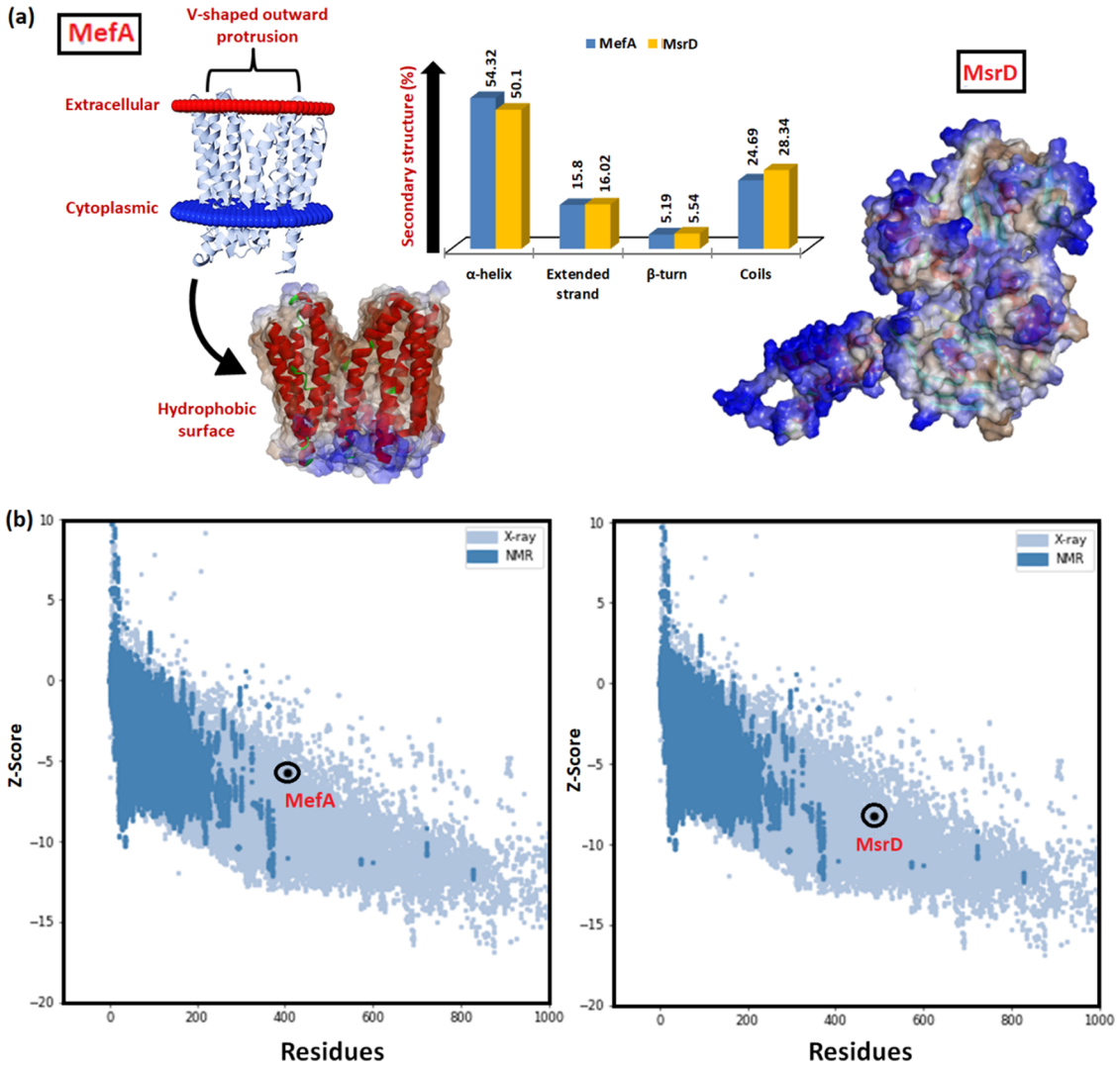

Figure 1. (a) MefA and MsrD structures with secondary structural patterns. (b) Comparison of predicted MefA and MsrD structures with experimental structures.

the same was not structurally characterized for a genotype-phenotype correlation study. The macrolide efflux protein of pneumococcus belongs to the major facilitator superfamily (MFS) and is 403 amino acids long. The protein shares >80% similarity with macrolide efflux protein MefA of *S. pyogenes* , and sometimes both these proteins are represented as MefA.[8] Similar homologues were detected in other bacteria as well (MefC in *Vibrio*, MefI in *S. pseudopneumoniae*, MefO in *S. dysgalactiae*, etc.). The presence of the *mefA* gene on macrolide efflux genetic assembly (MEGA) element, Tn2009, and Tn2010 transposons raises further concerns since they can easily be transmitted.[9] The transposons also carry an ABC-type transporter protein called MsrD that has two fused nucleotide-binding domains but no transmembrane domains. The genes MefE and MsrD are usually transcribed together and have macrolides as their inducers, especially the 14- and 15-membered macrolides.[10,11] The coexpression of both these genes is required for macrolide efflux in pneumococci, and they interact synergistically in *E. coli* with evidence of physical interactions. The expression of these genes is regulated by transcription attenuation.[12] The antiattenuation of transcription in the presence of macrolides leads to the expression of these genes. Despite its significance, the structure and mechanism of pneumococcal MefA-MsrD are not studied explicitly due to the dearth of a characterized structure. Our group has been ardently working on structural methods to compute antibiotic resistance mechanisms and therapeutic propositions.[13−16] We used standard computational methods to model the proteins followed by analyzing the interaction between the efflux-pump components MefA and MsrD. The mechanistic understanding of the MefA-MsrD interaction will give fair insight into MefA-MsrD-mediated macrolide interactions and encourage future therapeutic research.

2. RESULTS

2.1. Modeled Structure Validations and Stability Analyses. The predicted structure of the MefA protein predominantly consisted of α-helices with a central cavity (Figure 1). Subsequent refinement of protein structure resulted in an overall quality factor of 99.496 with no outliers in the Ramachandran plot. The predicted structure had membrane insertion energy within the range of transmembrane proteins with most of the residues having local quality >0.5. The structure, when embedded in the membrane, had a depth/hydrophobic thickness of 30.6 ± 1.1 Å and an average tilt of 8.0 ± 2.0° with $\Delta G_{transfer}$ of −90.4 kcal/mol. The embedded

https://doi.org/10.1021/acsomega.3c05210
ACS Omega 2023, 8, 39454−39467

and transmembrane residues are shown in Table 1. Majority of the 13 transmembrane segments comprised of embedded residues.

Table 1. Predicted Embedded and Transmembrane Residues in the MefE Modeled Structure

subunits	tilt (°)	segments
A	22	embedded residues:12−36, 39, 43−64, 67, 76−97, 100−124, 140−162, 164−187, 216, 224−246, 250, 253−274, 288−329, 331−332, 348−392
A	8	transmembrane segments:1(12−36), 2(43−64), 3(77−97), 4(102−124), 5(140−162), 6(167−186), 7(224−233), 8(237−247), 9(254−274), 10(290−305), 11(310−329), 12(348−373), 13(374−391)

From Figure 1a, it is evident that MefA and MsrD possessed higher percentages of helical patterns (>50%) and lesser proportions of strands (<17%) and turns (<6%). The quality of the structures adhered to the properties of X-ray diffraction and nuclear magnetic resonance-derived experimental protein structures having low *Z*-scores (<−5) (Figure 1 b).

The simulated trajectories of the proteins in water revealed local fluctuations in MsrD despite the low (<1 nm) average overall root-mean-square deviation (RMSD). MefA, however, displayed considerably equilibrated trajectory throughout the simulated time frame of 50 ns with a very low average RMSD (<0.5 nm) (Figure 2a). Similar patterns were evident in the root-mean-square fluctuation (RMSF) values. MsrD (RMSF < 0.7 nm) demonstrated higher local fluctuations than MefA (RMSF < 0.4 nm) (Figure 2a). The intramolecular H-bonds have been steadily maintained by the helical protein structures throughout the simulation time frame. Nevertheless, approximately 300 and 250 intramolecular H-bonds were observed in MsrD and MefA, respectively (Figure 2c). This inversely affected the overall (electron) density of the MsrD and MefA proteins, which equilibrated at 1005 and 1020 kg/m^3, respectively (Figure 2d). The helical barrel-shaped MefA had a uniformly compact radius of gyration (RoG) of <2.25 nm as compared to MsrD with RoG ∼3.25 nm (Figure 2e). The compactness of MefA entitled it with a lesser equilibrated overall solvent accessible surface area (SASA) of ∼200 nm^2 as compared to the uniform MsrD SASA of ∼280 nm^2 (Figure 2f).

Figure 3 shows the simulated MefA equilibrated in the dipalmitoylphosphatidylcholine (DPPC) membrane. The membrane-integrated MefA structure extracted at various intervals of the simulation displayed considerably low fluctuations (average RMSF < 0.8 Å) (Figure 3d). The simulated trajectory of MefA in the membrane revealed equilibrated pressure (∼0 bar) and average total energy (−2.4 × 10^6 kcal/mol) (Figure 4). However, SASA was reduced from ∼210 to ∼170 nm^2 as the protein was rendered in the membrane lipid bilayer (Figure 4b).

2.2. MefA-MsrD Interaction Dynamics. The interaction of MsrD with the cytoplasmic protrusion of MefA was carried out based on membrane-simulated MefA conformers extracted at different times, viz., 5, 10, 15, and 20 ns. Table 2 summarizes the overall interaction energetics based on statistically significant low-RMSD clusters comprising the lowest interaction energy, given as consensus HADDOCK scores. It was observed that the HADDOCK energy score was reduced in the interaction pose between MsrD and 20 ns conformer of MefA (−132.1 ± 9.5 kcal/mol) as compared to that of 5/10/15 ns MefA conformers (−105 ± 6.9, −107.0 ± 4.5, and −115.2 ± 6.3 kcal/mol respectively). The lowest energy pose was a part of the lowest RMSD cluster (0.7 ± 0.4 nm). The energy component comprised of considerable contributions from van der Waals energy, electrostatic energy, and desolvation energy functions. It was also observed that the lowest energy conformer possessed the highest buried surface area (2547.4 ± 97.3 nm^2), which can be correlated with the lowering of surface area in MefA observed in the previous section.

Figure 5 summarizes the energy components of the lowest cluster comprising the stable MefA-MsrD complex with the lowest energy. The mean restraint energy, electrostatic energy and the van der Waals energy were plotted alongside the other RMSD clusters (Figure 5a−c). Subsequently low-energy functions and low-interface RMSD profile plots justified choosing cluster 6 and obtaining the most energetically favorable MefA-MsrD complex (Figure 5d−i).

The lowest interaction energy conformer of the MefA-MsrD complex was attributed to 3 H-bonds and 38 hydrophobic interactions. Arg186, Glu190, and Lys165 of MefA elicited H-bonds with Ile59, Arg216, and Met48 of MsrD, respectively (Figure 6a). The lowest energy and intermolecular interactions were further reflected upon the comparatively low residue-level average RMSD profiles (<0.767) derived from coarse-grained simulations (Figure 6b).

2.3. Interaction of the Macrolides with MefA and MsrD. The binding energies of the conventional macrolides with MefA and MsrD revealed relative interaction potencies. Higher affinity of erythromycin toward both MefA (−3.73 kcal/mol) and MsrD (−5.85 kcal/mol) as compared to azithromycin (−5.39 and −2.95 kcal/mol) can be reflected upon the clinical susceptibilities of the drugs (Table 3). Both the drugs erythromycin (1.86 mM) and azithromycin (6.92 mM) revealed a high inhibition constant while interacting with the membrane component MefA as compared to the cytoplasmic ATP-binding counterpart MsrD.

The interaction of the macrolides with the ATP-binding domain of MsrD [InterPro ID: IPR003439, residues 5−196] justified the relative binding energies (Figure 7). The higher binding affinity (lower energy) correlates with more intermolecular interactions of erythromycin as compared to azithromycin. The MsrD interacting residues with each of the macrolides are different, and erythromycin has a slightly higher number of interactions (15 interactions) comprising H-bond and noncanonical interactions than azithromycin (13 interactions). Macrolides have very less propensity to interact with the cytoplasmic face of MefA protein via 5−7 interactions (H-bond/noncanonical interactions).

It was also observed from multiple sequence alignment that the interacting residues (Lys170, Tyr177, Asp171, Glu191, Gln195, Glu198, Gly396, Lys416, and Pro442) of MsrD with both macrolides are highly conserved across all of the major streptococcal species (Supplementary_file_1). The molecular dynamics simulation studies further revealed the similar interacting profiles of the macrolides with MsrD with minor differences (Figure 8). Low and stable interacting RMSD profiles for both drugs equilibrated at ∼0.5 nm. Their average RMSFs ranged between 0.25 and 0.5 nm. Slight compactness of azithromycin (average R_g ∼3.15 nm) over erythromycin (average R_g ∼3.30 nm) resulted in a slightly decreased SASA for the former (∼285 nm^2) as compared to the latter (∼295 nm^2). There were three consistent H-bonds for both the

https://doi.org/10.1021/acsomega.3c05210
ACS Omega 2023, 8, 39454−39467

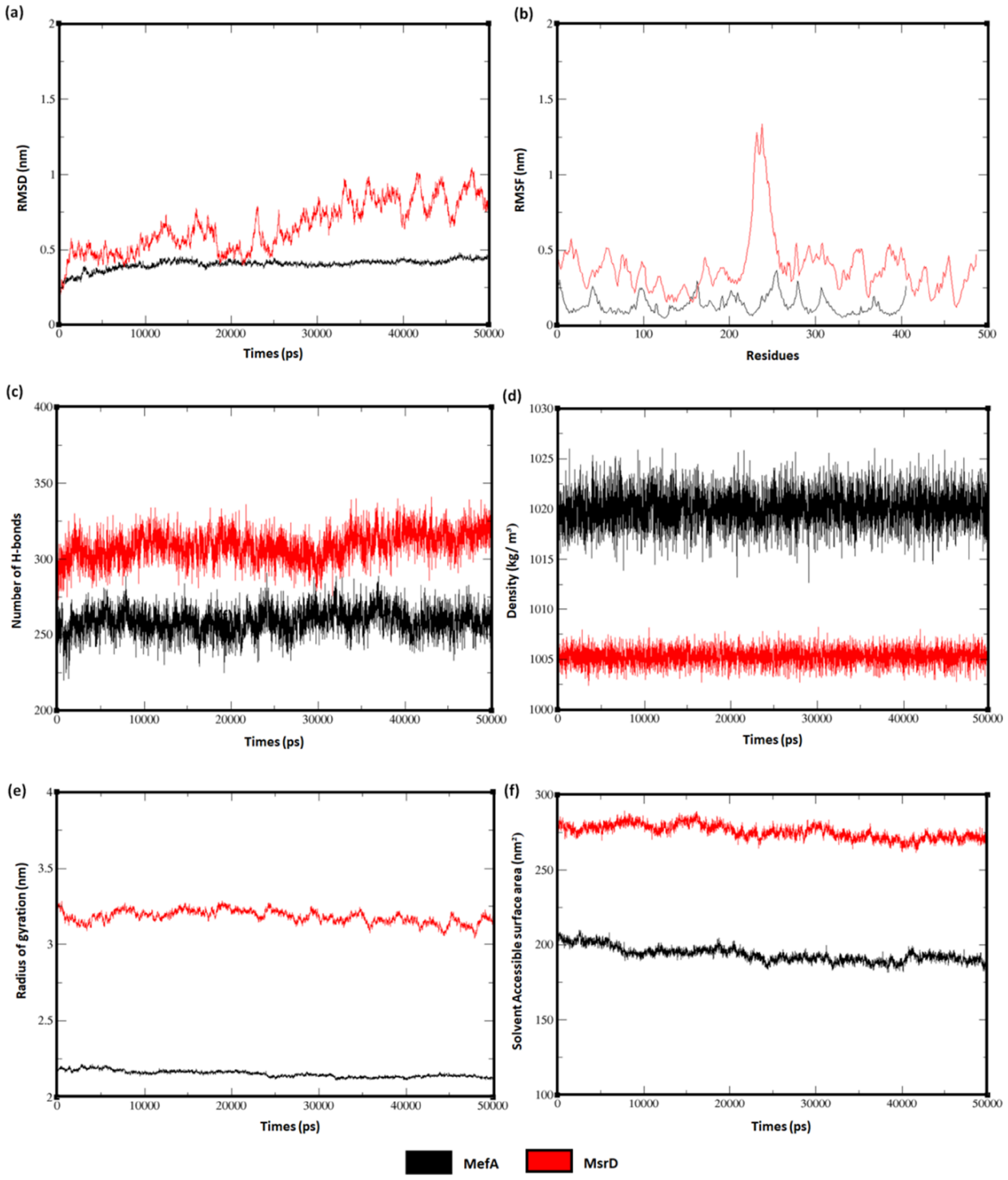

Figure 2. Simulation of the proteins in an aqueous environment. (a) RMSD, (b) RMSF, (c) number of H-bonds, (d) electron density, (e) RoG, and (f) SASA.

proteins formed during the 50 ns time frame. Finally, it was observed that the average linear interaction energy profiles of both the macrolide-MsrD complexes were fairly low (<0 kJ/mol), indicating reactive spontaneity. The lower IE profile of erythromycin than azithromycin further supported the docking energies.

3. DISCUSSION

Macrolides are frequently used to treat pneumonia and upper respiratory infections caused by *S. pneumoniae* ; however recently, macrolide resistance has become a significant issue.[12,18] Particularly in light of the COVID-19 pandemic and the widespread use of azithromycin as empiric treatment in COVID-19 patients in various parts of the world, macrolide resistance needs a thorough surveillance.[19] Since azithromycin is commonly available as an over the counter antibiotic in majority of the developing nations with high population density, it is confronted with substantial abuse and is a major cause of the exponential rise in macrolide resistance in recent years. In India, macrolide resistance in pneumococci has been

https://doi.org/10.1021/acsomega.3c05210
ACS Omega 2023, 8, 39454−39467

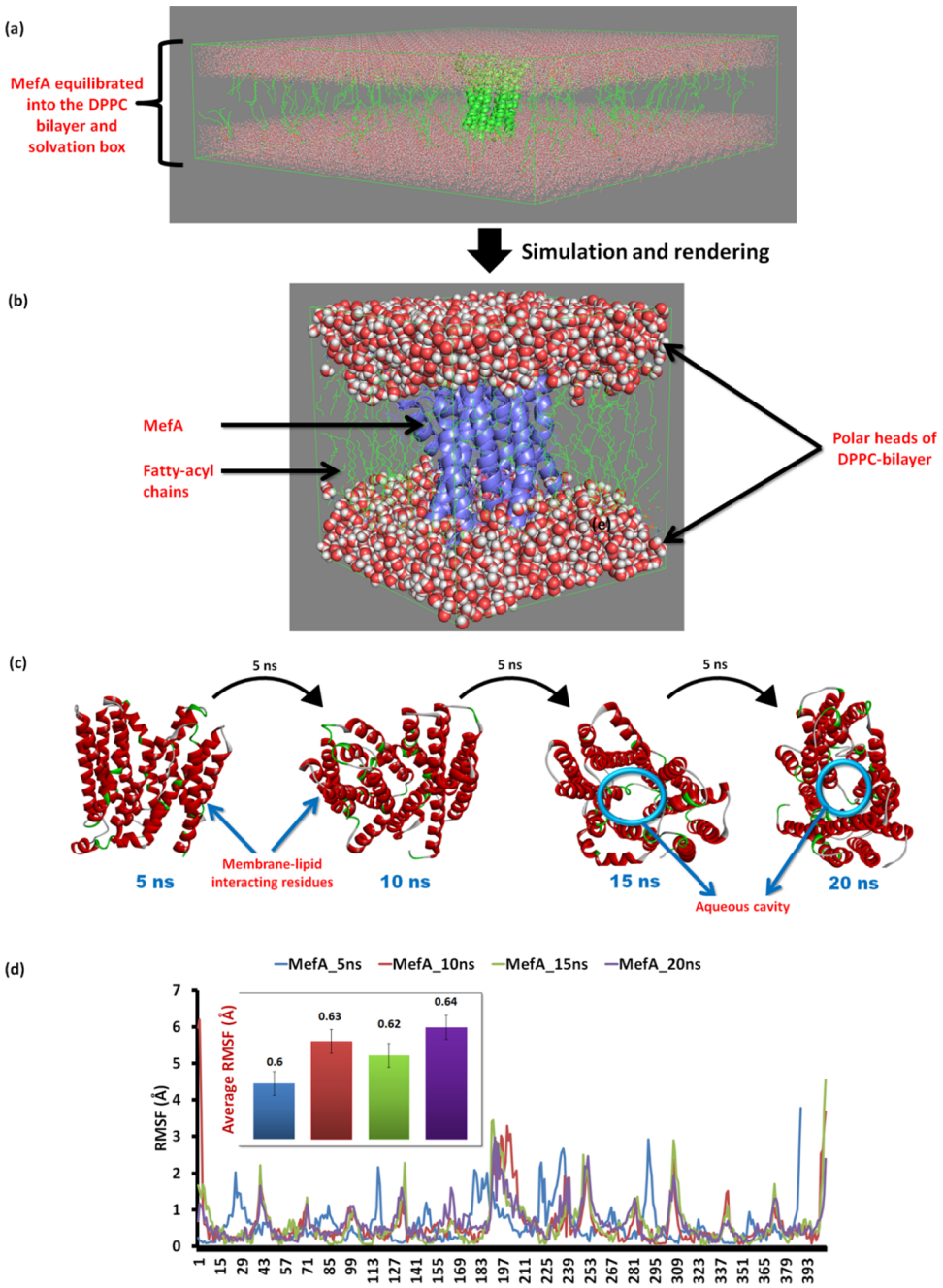

Figure 3. (a) Membrane-integrated equilibrated MefA protein. (b) Simulated and rendered MefA protein. (c) Simulated structures of MefA extracted at various intervals during the simulations. (d RMSFs of the simulated structures indicating the relative fluctuation changes during the simulation time frame.

increasing and currently is in the range of 20−35%.[6] Two commonly identified mechanisms in macrolide resistance are ribosomal methylation (*ermB*- mediated) and/or efflux of the drug (*mefA*-mediated).[12] Recent reports have highlighted the high mortality and vulnerability of infants to invasive pneumococcal disease, showing macrolide resistance. Interestingly, inclusion of the 13-valent pneumococcal conjugate vaccine (PCV13) reduced the MefA expression but retained macrolide resistance in *S. pneumoniae*.[19]

Efflux pumps are a frequently used detoxifying technique in biological systems. *Streptococcus pyogenes* (Group A *Streptococcus*) and *Streptococcus pneumoniae* both possess the MefA pump, which is encoded by the *mefA* gene and provides resistance to 14- and 15-membered macrolide antibiotics (such as erythromycin, azithromycin). Although there are many reports on efflux-pump inhibitors (EPIs) especially against the chromosomally encoded efflux pumps like AcrAB and NorA, the reports on plasmid/transposon encoded efflux pumps like MefA are rare. The main reason might be the narrow application domain.[20,21] However, the evolution of drug-resistant bacteria is unpredictably dynamic; moreover, due to considerable instances of *mefA*-mediated macrolide resistance in some parts of the world; it is always advantageous to enrich the therapeutic regime. Researchers have tried to extract marine secondary metabolites from >1000 crude extracts as MefA-EPIs; however dearth of a well-characterized MefA

https://doi.org/10.1021/acsomega.3c05210
ACS Omega 2023, 8, 39454−39467

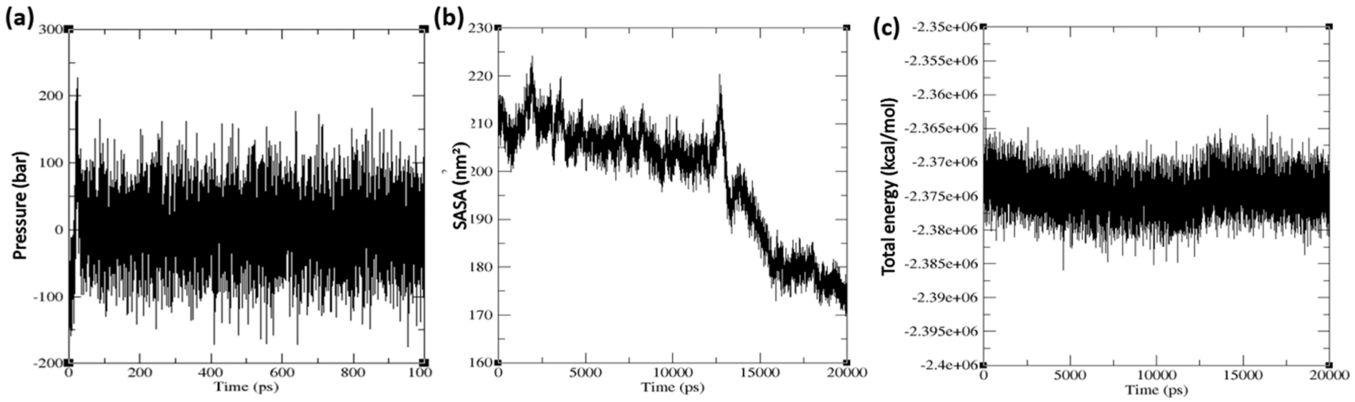

Figure 4. Simulated trajectories of MefA in the membrane (lipid) environment comprising integration of suitable water pockets. (a) Pressure, (b) SASA, and (c) total energy.

Table 2. Interaction Energetics of the Proteins Derived from the Best Clusters and Lowest-Energy Conformations

	MefA-MsrD complex			
properties	5 ns	10 ns	15 ns	20 ns
HADDOCK score (kcal/mol)	−105.0 ± 6.9	−107.0 ± 4.5	−115.2 ± 6.3	−132.1 ± 9.5
cluster size	14	17	20	10
RMSD (lowest energy structure) (nm)	14.9 ± 0.3	8.7 ± 0.1	21.4 ± 0.3	0.7 ± 0.4
van der Waals' energy (kcal/mol)	−70.8 ± 2.4	−54.8 ± 2.5	−62.9 ± 5.6	−80.3 ± 6.9
electrostatic energy (kcal/mol)	−88.5 ± 10.2	−149.8 ± 31	−187.1 ± 22.3	−95.2 ± 28.8
desolvation energy (kcal/mol)	−44.3 ± 1.4	−40.0 ± 3.9	−37.8 ± 5.4	−54.2 ± 1.6
restraint violation energy (kcal/mol)	277.2 ± 47.4	178.4 ± 37.2	229.4 ± 78.2	214.7 ± 37.2
buried surface area (nm^2)	2420.2 ± 81	2100.8 ± 131.7	2134 ± 115	2547.4 ± 97.3
Z-score	−1.5	−1.6	−2.2	−2.1
depth/hydrophobic thickness (Å)	30.4 ± 1.0	30.8 ± 0.7	30.4 ± 1.0	30.4 ± 1.0

structure imposed major challenges for the same. Fusidic acid derivatives, sulfated hydroquinones, agromycin, and pericidine A were proposed to be potent inhibitors, which needs thorough structural validations for a clinical translation.[22]

Over the last two decades, *mef*(*A*/*E*) and *mef*(*A*/*E*) + *erm*(*B*)-mediated macrolide resistance was found to be significantly high (50−75%) over *erm*-mediated macrolide resistance worldwide, especially in America and Europe, where *mef*(*A*/*E*) alone engendered >65% of macrolide resistance in *S. pneumoniae*. Macrolide resistance from *mef*(*A*/*E*) in *S. pyogenes* was also considerably high in Africa (>48%), Europe (>40%), and Asia (∼40%).[23] It was discovered that the *mef*(*A*) − *msr*(*D*) tandem is a required hallmark for the development of an active efflux transport system. The *mefA*/*E* and *msrD* genes are typically present in an operon located in the MEGA. The operon is translated as a polycistronic mRNA (in the presence of erythromycin) from a single promoter that is situated around 350 bp upstream of the *mefA* gene.[24] The *mef*(*A*) gene is often carried into phage φ1207.3. The transposon Tn1207.1, associated with the international clone England[14]-ST9, majorly governs the spread of the *mef*(*A*) gene in pneumococci. The MEGA, on the other hand, carries the *mef*(*E*) gene as a *mef*(*E*) − *mrs*(*D*) tandem that may also be incorporated into larger structures holding additional resistance determinants.[10,25,26] Experimental reports suggest that the deletion of MsrD rather than MefA profoundly reduced macrolide (erythromycin) efflux in *S. pneumoniae*.[27] For a detailed research on the mechanism of the MefA-MsrD-mediated resistance, it is imperative to have well-characterized structures of the proteins and their physical interaction profiles with each other as well as the macrolide antibiotics. The dearth of available structures compelled us to formulate the protein models using a combination of homology modeling, threading, and dynamics. For this purpose, we considered global genome projects as well as multispecies protein sequences (accession ID: WP_000417519.1). The proteins showed high sequence identity (>90%) among the *Streptococcus* sp. through BLAST-search profiles. The finding adheres to previous reports suggesting high similarity of the efflux proteins among the *Streptococcus* genus.[28] Structural profiles of the modeled proteins adhered to quality parameters (high quality score >97; Ramachandran favored regions >98%) as described in previous studies and were highly stable based on their consistent simulation trajectories.[29−32]

These proteins operate with two intermediate states−the inward facing (C_i) and the occluded (C_o) conformations. The MefA is similar to the C_i conformation of GlpT with two domains.[33] A central cavity is present throughout the protein and perhaps the channel for drug efflux. The 13 helices are embedded in the lipid bilayer and were further simulated in the membrane to achieve a more compact structure with minimal overall fluctuations. The overall pressure and energy of the MefA system were uniform, asserting the thermodynamic stability of the MefA protein integrating into the membrane.

The physical associations of MefA and MsrD were determined by subjecting their simulated structures to protein−protein docking. The lowest energy and low RMSD pose of the MefA-MsrD complex indicated consistently low structural fluctuation derived from coarse-grained dynamics and hence were interacting stably. Finally, the interaction of the antibiotics was evaluated for both the proteins. It was evident that both the macrolides, especially erythromycin, have

https://doi.org/10.1021/acsomega.3c05210
ACS Omega 2023, 8, 39454−39467

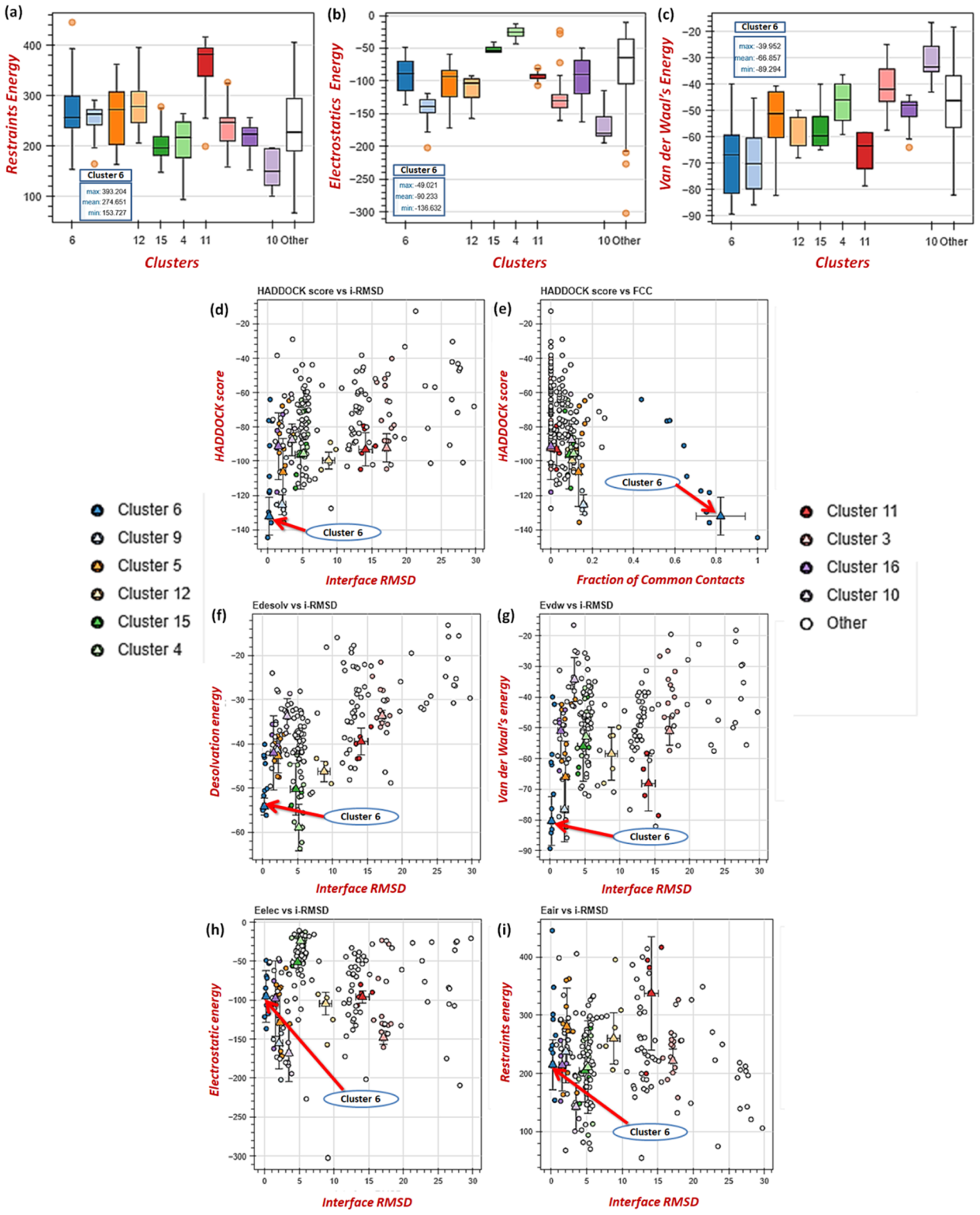

Figure 5. Energetics of the MefA-MsrD complex clusters. (a) Restraint energy of the clusters, (b) electrostatic energy of the clusters, (c) van der Waals energy of the clusters, (d) HADDOCK score vs RMSD, (e) HADDOCK score vs FCC, (f) desolvation energy vs RMSD, (g) vdW energy vs RMSD, (h) electrostatic energy vs RMSD, and (i) restraint energy vs RMSD.

higher affinity toward interacting with MsrD as compared to MefA. Intermolecular interactions in the docked structures supported the binding energy scores and dissociation constants indicating the higher relevance of MsrD in macrolide interaction than MefA in *S. pneumoniae* which correlates with previous studies.[27] It was also observed that the macrolide interacting residues in MsrD proteins are highly conserved in all streptococcal species (Supplementary_file_1), and hence, it is prone to affect pan-species susceptibility of macrolides. Molecular dynamics simulations ascertained the stable interaction of the macrolides with MsrD. The local fluctuation in the RMSF was characterized by transient H-bonds formed

https://doi.org/10.1021/acsomega.3c05210
ACS Omega 2023, 8, 39454−39467

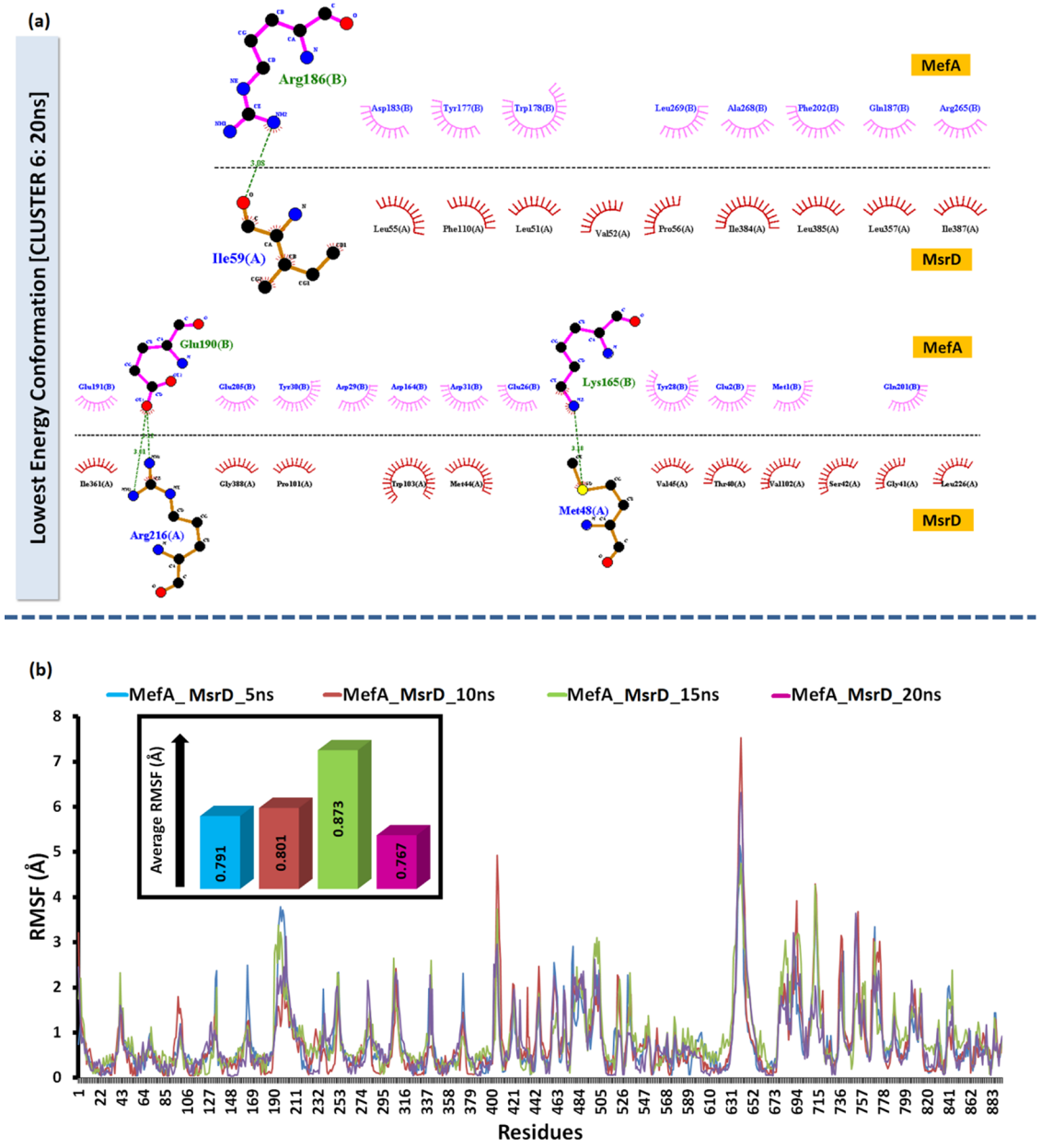

Figure 6. (a) Intermolecular interaction of the lowest-energy conformer of Mef-MsrD complex. (b) RMSF profiles of the lowest-energy structures.

Table 3. Macrolide Interaction Profile with the Target Proteins

drugs	susceptible MIC values[a] (μg/mL)	target proteins	binding energy (kcal/mol)	inhibition/ dissociation constant (mM)
erythromycin	≤0.25	MsrD	−5.85	0.05
		MefA	−3.73	1.86
azithromycin	≤0.50	MsrD	−5.39	0.11
		MefA	−2.95	6.92

[a]As per Clinical and Laboratory Standards Institute (CLSI) guidelines.[17]

between MsrD and antibiotics (Figure 8). However, the overall average RMSF was fairly low (<1 nm), which depicts considerable stability in protein drug interactions.[34,35] Although the interaction dynamics of erythromycin and azithromycin with MsrD is similar (<5% difference in RMSD and RMSF), the latter due to its extended functional groups manages to result in more compaction of the MsrD structure than erythromycin. The same is reflected upon the SASA as compaction reduces the solvent accessibility. The higher MIC of azithromycin as compared to erythromycin can be mediated by the slower efflux of the latter resulted by higher propensity of interacting with cytoplasmic MsrD. Since the interaction with the antibiotics and protein−protein association are occurring at different sites and unaffected by each other, future antimicrobials can be designed either to prevent MefA-MsrD association and/or masking interactive potentials with MsrD.

Researchers have explored potential FDA-approved EPIs against clinical *Staphylococcus aureus*, as well as natural compounds to target MefA/E-pumps in drug-resistant bacteria; however, the same were not translated clinically.[36−38] The structural insights from the present study can be instrumental in phenotypic studies on macrolide resistance in

https://doi.org/10.1021/acsomega.3c05210
ACS Omega 2023, 8, 39454−39467

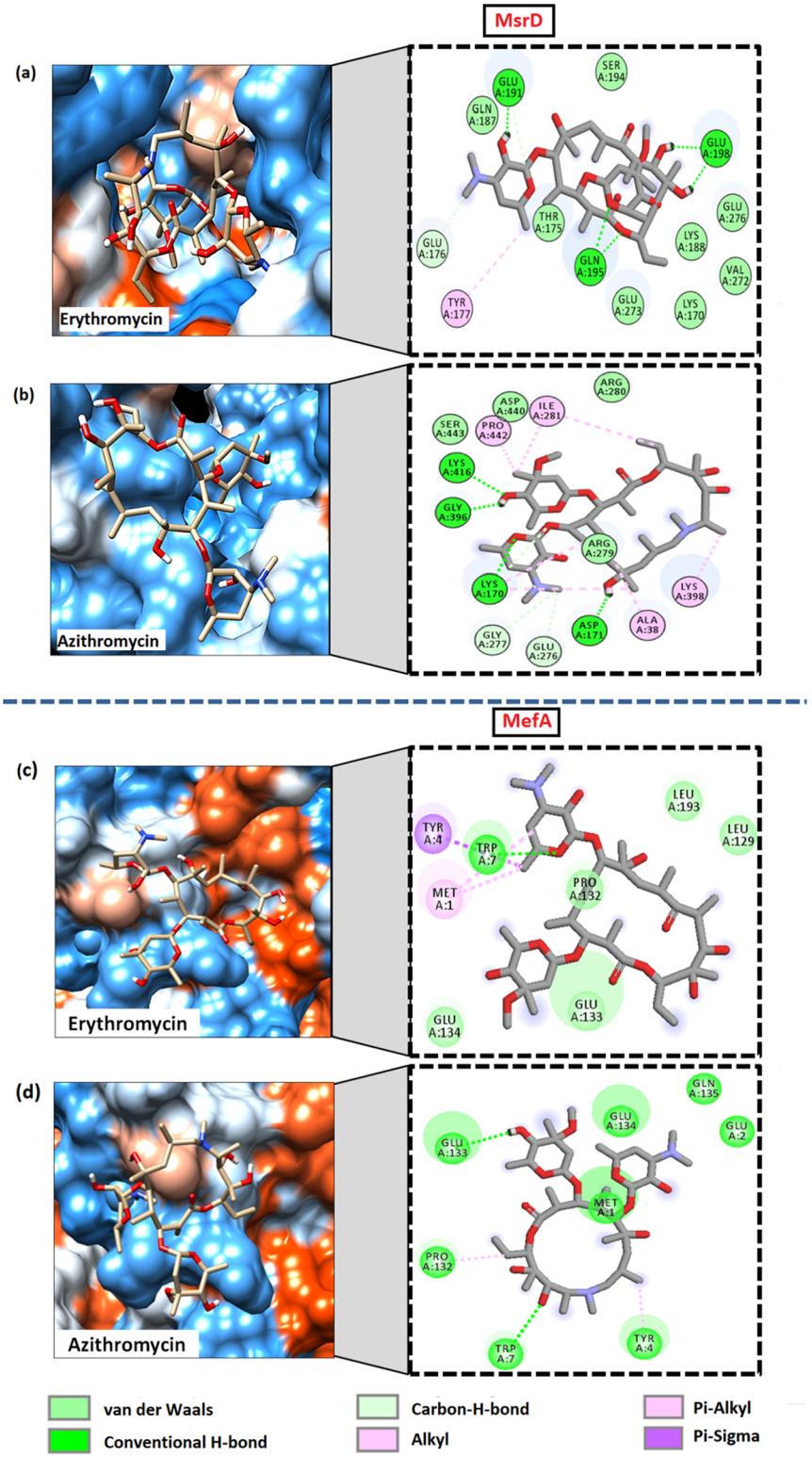

Figure 7. Intermolecular interactive pattern of macrolides with targets. (a) MsrD + erythromycin, (b) MsrD + azithromycin, (c) MefA + erythromycin, and (d) MefA + azithromycin.

pneumococci and also in designing potent EPIs translatable to the clinics.

4. CONCLUSIONS

MefA-MsrD primarily governs macrolide efflux in pathogenic pneumococci. In the present study, the macrolide efflux-protein complex MefA-MsrD was successfully modeled and validated by using standard computational tools. MefA orientation in the membrane was found to possess typical MFS superfamily like structure with 13 transmembrane spans and a V-shaped conformation. The proteins were subjected to multiple simulation cycles in membrane and cytoplasmic environments to achieve their stable conformations in ideal

https://doi.org/10.1021/acsomega.3c05210
ACS Omega 2023, 8, 39454−39467

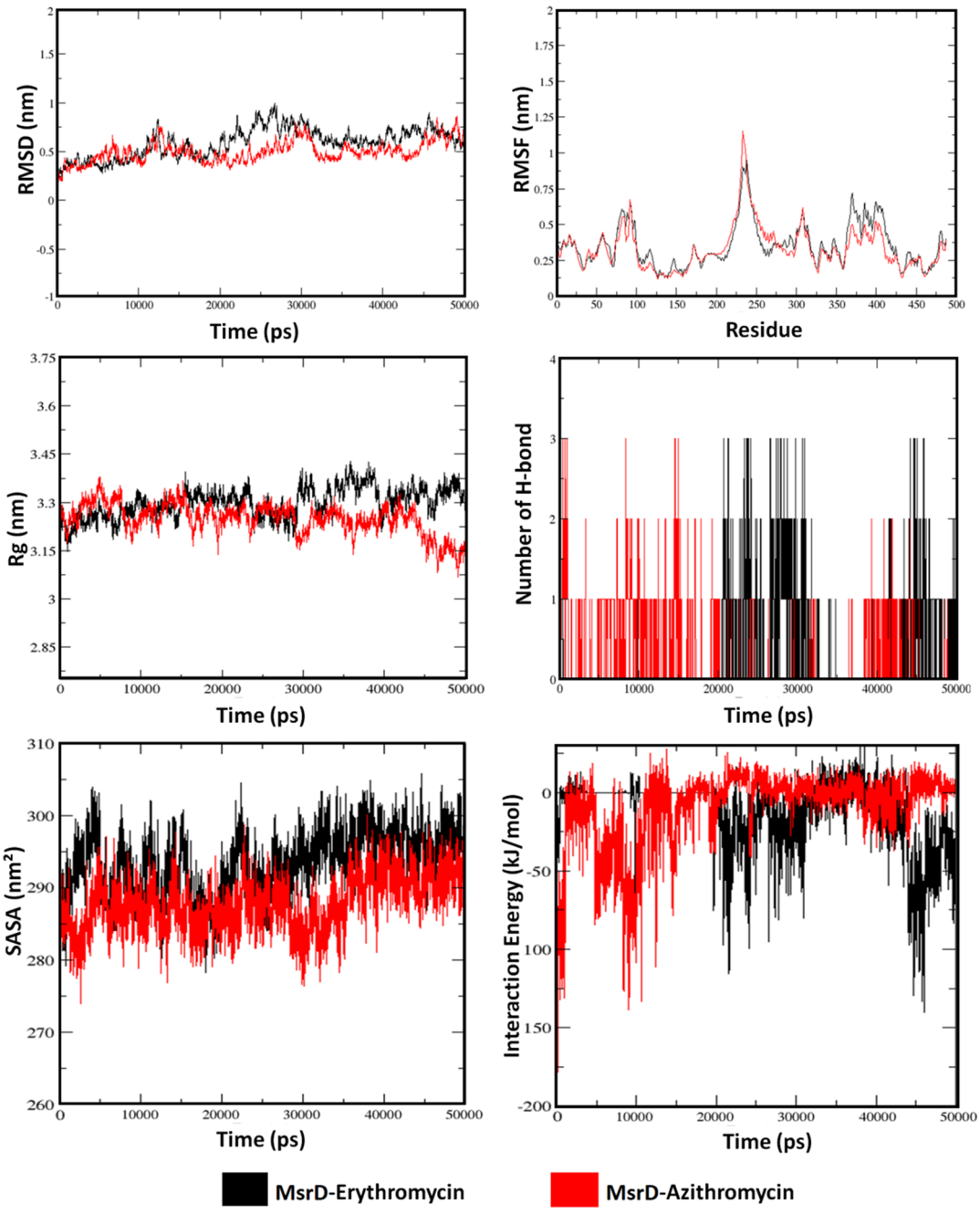

Figure 8. MDS trajectories of MsrD interacting with erythromycin (black) and azithromycin (red) depicting RMSD, RMSF, RoG (Rg), number of H-bonds, SASA, and interaction energies.

environments. The physical association of the proteins was determined by deriving the lowest energy conformer of the MefA-MsrD complex. The interaction dynamics of the antibiotics were unaffected by the physical interaction of the proteins. MsrD showed a higher propensity in interacting with the macrolides than MefA, hence validating the greater significance of the former in macrolide resistance. The study is probably the first structural report on pneumococcal MefA-MsrD complexes and associated macrolide resistance, which provides leads for future therapeutic designs.

5. METHODS

5.1. Protein Data Set. The MefA and MsrD coding sequences (CDS) were retrieved from the '*S. pneumoniae* global lineages' [accession ID: PRJEB2255] from the National Centre for Biotechnology Information (NCBI) database (https://www.ncbi.nlm.nih.gov/). The initial BLASTp search with the CDS in the "Protein data bank" revealed no similar structures; however, "nonredundant databases" revealed sequences available for MefA (Uniprot ID: A0A2K9YNE2) and MsrD (Uniprot ID: B1B649) with an identity of 100% but incomplete coverage. Therefore, sequences retrieved from global lineages were selected for modeling.

5.2. Protein Modeling, Structural Optimization, and Validations. The lack of available 3D structures of MefA and MsrD proteins invoked us to model the proteins as per our previous studies, combining homology and ab initio approach.[39,40] The qualities as well as stability of the structures

https://doi.org/10.1021/acsomega.3c05210
ACS Omega 2023, 8, 39454−39467

were ensured by multiple validation steps and simulations, as described subsequently.

5.2.1. Protein Modeling and Optimization. Swiss-Model (https://swissmodel.expasy.org/), Robetta (https://robetta.bakerlab.org/), and Modeler were used to generate suitable templates.[41,42] The protein structures were refined using the GalaxyRefine server (https://galaxy.seoklab.org/) by reducing clash scores, poor rotamers, and percentage Ramachandran outliers and minimizing side-chain rotamers.[43] Finally, 2000 steps of the steepest descent and conjugate gradient algorithms using Swiss-PDB viewer (SPDBV) with the GROMOS96 43B1 force-field *in-vacuo* were used to minimize the energy of the structures.[44] Thus, the target protein architectures were improved in accordance with earlier studies.[15,31,45] By determining the stereochemical characteristics of the residues falling in the permitted regions (>95%) of the Ramachandran plot having least unfavorable angles with the highest overall model score, the models were validated using the MolProbity tool (http://molprobity.biochem.duke.edu/index.php) and Procheck (https://saves.mbi.ucla.edu/).[46,47] SOPMA web-tool (https://npsa-prabi.ibcp.fr/cgi-bin/npsa_automat.pl?page=/NPSA/npsa_sopma.html) was used to determine the proteins' secondary structural patterns.[48] The orientation of the protein in the membrane was estimated using OPM (Orientation of Proteins in Membranes) server.[49] All final images were downloaded from the respective sites, and protein structure visualization was performed in DISCOVERY STUDIO. The most suitable proteins were finalized based on model quality profiles.

5.2.2. Molecular Dynamics Simulation. The modeled proteins were further optimized and validated for intrinsic stability by simulating them using the GROMACS suite. The simulations were carried out in cytosolic (aqueous) as well as membrane (lipid-bilayer) environments to provide ideal conditions for the proteins for stabilizing themselves in their respective cellular locations.

5.2.2.1. Aqueous Environment Simulations. To obtain the considerably stable forms of both MefA and MsrD, they were simulated in an aqueous environment for a 50,000 ps time scale using GROMACS 2020.1 suite.[50,51] CHARMM36-2019 all-atom force-field was used to build the requisite macromolecular topology followed by solvation with a straightforward point-charge TIP3 water model and neutralizing the system by adding the necessary counterions (Na+ or Cl+). The protein was centrally placed in a dodecahedron box with a uniform edge distance (1.5 nm) during simulation.[50] Energy minimization was accomplished using the steepest descent algorithm, which included 50,000 steps and a tolerance for convergence of 1000 kJ/mol/nm. For 150 ps, equilibrations were carried out using the typical NVT (constant number of particles, volume, and temperature) and NPT (constant number of particles, pressure, and temperature) ensembles. After the Parrinello−Rahman extended coupling ensemble was used for pressure scaling, long-range electrostatic interactions with an order of 4.0 and a Fourier spacing of 0.16 nm were treated using particle-mesh Ewald electrostatics summation. The RMSF, R_g, SASA, and RMSD curves were used to interpret the relative overall dynamics (and stability) of the wild-type and mutant proteins.[45,52]

5.2.2.2. Lipid-Bilayer Environment Simulations. The MefA protein being a membrane protein was thereafter simulated in a membrane-lipid environment using simulated (DPPC) bilayer comprising Ryckaert-Bellemans dihedral potentials. A hybrid mode between GROMOS atom types and OPLS partial charges were adopted to construct the topology. GROMOS53a6_lipid force-field (with Berger lipid parameters) was selected to poise the protein−membrane integrate encompassing bonded and nonbonded parameters. Energy minimization of 50,000 steps with the steepest decent algorithm (cutoff force <1000 kg/mol/nm) was performed followed by multiple iterations of "shrinking" to estimate the area per lipid. 100 and 100 ps of NVT and NPT equilibrations respectively were carried out using solvated protein−membrane system using the Nose-Hoover thermostat for accurate kinetic ensembles and semi-isotropic pressure scaling. Simulation was carried out with Parrinello−Rahman extended pressure-coupling ensemble, long-range electrostatic interactions with an order of 4.0, Fourier spacing of 0.16 nm, and particle-mesh Ewald electrostatics summation. The simulated properties were determined as mentioned in the previous section.[53]

5.3. Protein−Protein Interaction. The physical interaction between MefA and MsrD was derived from flexible protein−protein docking using a clustering algorithm, followed by determining residue level fluctuation profiles. MefA protein structures, at various intervals (5, 10, 15, and 20 ns) from its membrane simulation poses and simulated MsrD structure (50 ns), were taken.

5.3.1. Clustering-Based Protein−Protein Docking. The MefA-MsrD interactions were determined using the simulated structures through HADDOCK web-interface (https://wenmr.science.uu.nl/haddock2.4/). The information-driven flexible docking method HADDOCK (High Ambiguity Driven Protein−protein DOCKing) was used to model the protein complexes at suitable sites. HADDOCK involves ab initio docking techniques by utilizing ambiguous interaction restraints to carry out the docking process by considering known or expected protein interfaces as reference. It also accommodates a number of other experimental data, such as NMR residual dipolar couplings, pseudo contact shifts, and cryo-EM maps, and enables the construction of precise, unambiguous distance restrictions (for instance, using MS cross-links). The lowest energy structures are derived from a consolidation of multiple energy functions. The structures and intermolecular interactions of the docked complexes were visualized with Chimera and LigPlot+, respectively.[54,55]

5.3.2. Coarse-Grained Dynamics Simulation. Coarse-grained dynamics simulation of the protein−protein complexes was performed to ascertain the overall structural fluctuation (stability) of the MefA-MsrD complexes with CABSflex interface (http://biocomp.chem.uw.edu.pl/CABSflex2/). The maximum and minimum boundaries to pair atoms within defined spaces during simulations were restrained with default parameters. Restraining prevented unstable conformations with deviations beyond assigned ranges. The default settings and restraints were optimized to merge coarse dynamics simulations and consensus protein fluctuations in aqueous environment derived by all-atom molecular dynamics simulation (10 ns time scale with suitable force-fields). The default parameters were selected with restrain gap = 3 (minimum distance between previous and next amino acid in the chain to be restrained) and minimum and maximum conformational distances of 3.8 and 8.0 Å, respectively. The flexibilities were analyzed from the RMSF values generated.[56] The relative RMSF of the protein−protein complexes gave insight into their interaction dynamics.

https://doi.org/10.1021/acsomega.3c05210
ACS Omega 2023, 8, 39454−39467

5.4. Macrolide Interaction. The interaction of the macrolides with both the proteins was determined to check the relative affinities, dissociation constants, and intermolecular interactions.

5.4.1. Macrolide Structure Retrieval. The standard antibiotic molecules viz. erythromycin (ID: 12560) and azithromycin (ID: 447043) were obtained from the PubChem database (https://pubchem.ncbi.nlm.nih.gov/) in SDF formats. 3D formatting of the antibiotics prior to docking was achieved using the OpenBabel tool. The antibiotics/drugs have been synonymously referred to as 'ligand' in the present study.

5.4.2. Molecular Docking. The relative binding potential of the simulated MsrD and MefA with standard antibiotics (erythromycin and azithromycin) was examined by molecular docking using AutoDock4.0 and embedded tools.[57] Prior to docking analysis, the crystallographic water molecules and unwanted heteroatoms were removed from the structure of the target proteins. The proteins in ideal geometry were optimized by adding polar hydrogen atoms and merging nonpolar hydrogen atoms. Requisite Kollman charges were added to stabilize the protein structures. The torsions were fixed, and Gasteiger charges were added for the ligand. The initial parameters and van der Waals well depth of 0.100 kcal/mol were assigned for the protein, and the files were saved in PDBQT files format. The grid box was centered at crucial functional domains identified from previous literature and was constructed with appropriate dimensions to include the entire domain. The drug-binding pockets were further validated from the INTERPRO and CASTp (http://sts.bioe.uic.edu/castp/index.html?2011) servers. The AutoDock tools were used to generate grid parameter files and docking parameter files. Finally, the Lamarckian genetic algorithm generated possible target proteins and ligand complexes in compatible conformations. The top-ranked complexes based on the lowest binding energies (highest affinities) were visualized using LigPlot[55] and Discovery Studio.[58] The intermolecular interactions of the complexes were analyzed to determine the crucial residues of the target that can contribute to the drug binding.[52,59−61]

5.4.3. Molecular Dynamics Simulation. The docked complexes with high binding affinities were simulated for 50,000 ps. GROMACS 2021.2 package with CHARMM36-Mar2019 force-field mechanics and the TIP3P model (for the water cluster) was used. The ligand topology was built using the CGenFF server. To carry out the protein−ligand complex simulation, we placed the complex in the center of a dodecahedron box with a uniform edge distance of 1.0 nm. Particle mesh Ewald electrostatics summation was used for treating long-range electrostatic interactions with an order of 4.0 and a Fourier spacing of 0.16 nm. Parrinello−Rahman extended coupling ensemble was used for pressure scaling by applying motion equations to the box vectors. The free energy profile in the protein ligand complexes was validated with the linear interaction energy module of GROMACS. The interaction energies of the entire simulation trajectory were extracted by a rerun of 10 ns by including short-range and long-range Coulombic energy functions.

■ ASSOCIATED CONTENT

Data Availability Statement

The data associated with the manuscript are available in the manuscript and/or supplementary file.

Supporting Information

The Supporting Information is available free of charge at https://pubs.acs.org/doi/10.1021/acsomega.3c05210.

MSA of MsrD (Mel) in different *Streptococcal* species (PDF)

■ AUTHOR INFORMATION

Corresponding Authors

Sujatha Sistla − *Department of Microbiology, Jawaharlal Institute of Postgraduate Medical Education and Research (JIPMER), Puducherry 605006, India*; Email: sujathasistla@gmail.com

Paul Livingstone − *Department of Sports and Health Sciences, Cardiff Metropolitan University, Cardiff CF5 2YB, U.K.*; Email: PGLivingstone@cardiffmet.ac.uk

Anand Anbarasu − *Medical and Biological Computing Laboratory, School of Biosciences and Technology, Vellore Institute of Technology (VIT), Vellore 632014 Tamil Nadu, India*; orcid.org/0000-0003-2216-7488; Email: aanand@vit.ac.in

Authors

Sreeram Chandra Murthy Peela − *Department of Microbiology, Jawaharlal Institute of Postgraduate Medical Education and Research (JIPMER), Puducherry 605006, India*

Soumya Basu − *Medical and Biological Computing Laboratory, School of Biosciences and Technology, Vellore Institute of Technology (VIT), Vellore 632014 Tamil Nadu, India*

Jyoti Sharma − *Department of Bioscience and Bioengineering, Indian Institute of Technology (IIT), Jodhpur 342011 Rajasthan, India*

Abdullah F. AlAsmari − *Department of Pharmacology and Toxicology, College of Pharmacy, King Saud University, Riyadh 11451, Saudi Arabia*

Fawaz AlAsmari − *Department of Pharmacology and Toxicology, College of Pharmacy, King Saud University, Riyadh 11451, Saudi Arabia*

Sultan Alalmaee − *InterHealth Hospital, Riyadh 12371, Saudi Arabia*

Sudha Ramaiah − *Department of Biosciences, Vellore Institute of Technology (VIT), Vellore 632014 Tamil Nadu, India*; orcid.org/0000-0002-4800-329X

Complete contact information is available at: https://pubs.acs.org/10.1021/acsomega.3c05210

Author Contributions

S.M.P. and S.B.: study design, investigation, formal analysis, visualization, and writing—original draft preparation. J.S.: formal analysis and visualization. A.A., F.A., S.A., and S.R.: methodology, validation, and writing—review and editing. P.L., S.S., and A.A.: conceptualization, supervision, resources, and writing—review and editing. S.C.M.P. and S.B. contributed equally as joint first authors.

Funding

The authors are thankful to the researchers supporting project number (RSP2023R235), King Saud University, Riyadh, Saudi Arabia.

Notes

The authors declare no competing financial interest.

■ ACKNOWLEDGMENTS

The authors would like to acknowledge the Management of VIT, Vellore for the technical support. S.C.M.P. is grateful to ICMR, New Delhi for the Research Associateship (OMI-Fellowship/3/2020-ECD-I). The authors would also like to acknowledge the ICMR, New Delhi for research grant IRIS ID 2021-10630.

■ REFERENCES

(1) World Health Organization. *Pneumococcal Disease*. https://www.who.int/teams/health-product-policy-and-standards/standards-and-specifications/vaccine-standardization/pneumococcal-disease.

(2) Bertran, M.; Amin-Chowdhury, Z.; Sheppard, C. L.; Eletu, S.; Zamarreño, D. V.; Ramsay, M. E.; Litt, D.; Fry, N. K.; Ladhani, S. N. Increased Incidence of Invasive Pneumococcal Disease among Children after COVID-19 Pandemic, England. *Emerg. Infect. Dis.* **2022**, *28* (8), 1669−1672.

(3) Amin-Chowdhury, Z.; Bertran, M.; Sheppard, C. L.; Eletu, S.; Litt, D.; Fry, N. K.; Ladhani, S. N. Does the Rise in Seasonal Respiratory Viruses Foreshadow the Return of Invasive Pneumococcal Disease This Winter? *Lancet. Respir. Med.* **2022**, *10* (1), e1−e2.

(4) Anandan, S.; Sethuvel, D. P. M.; Gajendiren, R.; Verghese, V. P.; Walia, K.; Veeraraghavan, B. Molecular Characterization of Antimicrobial Resistance in Clinical Shigella Isolates during 2014 and 2015: Trends in South India. *Germs* **2017**, *7* (3), 115−122.

(5) Shaeer, K. M.; Chahine, E. B.; Varghese Gupta, S.; Cho, J. C. Macrolide Allergic Reactions. *Pharmacy* **2019**, *7* (3), 135.

(6) Peela, M. S. R.; Sistla, S.; Tamilarasu, K.; Krishnamurthy, S.; Adhisivam, B. Antimicrobial Resistance in Clinical Isolates of Streptococcus Pneumoniae: Mechanisms and Association with Serotype Patterns. *J. Clin. Diagnostic Res.* **2018**, *12*, 17 DOI: 10.7860/JCDR/2018/37414.12287.

(7) Canu, A.; Malbruny, B.; Coquemont, M.; Davies, T. A.; Appelbaum, P. C.; Leclercq, R. Diversity of Ribosomal Mutations Conferring Resistance to Macrolides, Clindamycin, Streptogramin, and Telithromycin in Streptococcus Pneumoniae. *Antimicrob. Agents Chemother.* **2002**, *46* (1), 125−131.

(8) Roberts, M. C.; Sutcliffe, J.; Courvalin, P.; Jensen, L. B.; Rood, J.; Seppala, H. Nomenclature for Macrolide and Macrolide-Lincosamide-Streptogramin B Resistance Determinants. *Antimicrob. Agents Chemother.* **1999**, *43* (12), 2823−2830.

(9) Fyfe, C.; Grossman, T. H.; Kerstein, K.; Sutcliffe, J. Resistance to Macrolide Antibiotics in Public Health Pathogens. *Cold Spring Harb. Perspect. Med.* **2016**, *6* (10), No. a025395.

(10) Ambrose, K. D.; Nisbet, R.; Stephens, D. S. Macrolide Efflux in Streptococcus Pneumoniae Is Mediated by a Dual Efflux Pump (Mel and Mef) and Is Erythromycin Inducible. *Antimicrob. Agents Chemother.* **2005**, *49* (10), 4203−4209.

(11) Nunez-Samudio, V.; Chesneau, O. Functional Interplay between the ATP Binding Cassette Msr(D) Protein and the Membrane Facilitator Superfamily Mef(E) Transporter for Macrolide Resistance in Escherichia Coli. *Res. Microbiol.* **2013**, *164* (3), 226−235.

(12) Schroeder, M. R.; Stephens, D. S. Macrolide Resistance in Streptococcus Pneumoniae. *Front. Cell. Infect. Microbiol.* **2016**, *6*, 98.

(13) Naha, A.; Vijayakumar, S.; Lal, B.; Shankar, B. A.; Chandran, S.; Ramaiah, S.; Veeraraghavan, B.; Anbarasu, A. Genome Sequencing and Molecular Characterisation of XDR Acinetobacter Baumannii Reveal Complexities in Resistance: Novel Combination of Sulbactam−Durlobactam Holds Promise for Therapeutic Intervention. *J. Cell. Biochem.* **2021**, *122* (12), 1946−1957.

(14) Debroy, R.; Ramaiah, S. MurC Ligase of Multi-Drug Resistant Salmonella Typhi Can Be Inhibited by Novel Curcumin Derivative: Evidence from Molecular Docking and Dynamics Simulations. *Int. J. Biochem. Cell Biol.* **2022**, *151*, No. 106279.

(15) Basu, S.; Varghese, R.; Debroy, R.; Ramaiah, S.; Veeraraghavan, B.; Anbarasu, A. Non-Steroidal Anti-Inflammatory Drugs Ketorolac and Etodolac Can Augment the Treatment against Pneumococcal Meningitis by Targeting Penicillin-Binding Proteins. *Microb. Pathog.* **2022**, *170* (July), No. 105694.

(16) Basu, S.; Joshi, S. M.; Ramaiah, S.; Anbarasu, A. Designing Anti-Microbial Peptides Against Major β-Lactamase Enzymes in Clinically Important Gram-Negative Bacterial Pathogens: An In-Silico Study. *Probiotics Antimicrob. Proteins* **2022**, *14* (2), 263−276.

(17) Clinical and Laboratory Standards Institute (CLSI). *Methods for Antimicrobial Dilution and Disk Susceptibility Testing of Infrequently Isolated or Fastidious Bacteria*. 3rd Ed.; Clinical and Laboratory Standards Institute: Wayne, PA, CLSI Doc. M45, 2021.

(18) Tsuzuki, S. Macrolide Resistance in Streptococcus Spp. *Lancet Infect. Dis.* **2019**, *19* (3), 243−244.

(19) Gonzales, B. E.; Mercado, E. H.; Pinedo-Bardales, M.; Hinostroza, N.; Campos, F.; Chaparro, E.; Del Águila, O.; Castillo, M. E.; Saenz, A.; Reyes, I.; Ochoa, T. J. Increase of Macrolide-Resistance in Streptococcus Pneumoniae Strains After the Introduction of the 13-Valent Pneumococcal Conjugate Vaccine in Lima, Peru. *Front. Cell. Infect. Microbiol.* **2022**, *12*, 12.

(20) Lomovskaya, O.; Warren, M. S.; Lee, A.; Galazzo, J.; Fronko, R.; Lee, M.; Blais, J.; Cho, D.; Chamberland, S.; Renau, T.; Leger, R.; Hecker, S.; Watkins, W.; Hoshino, K.; Ishida, H.; Lee, V. J. Identification and Characterization of Inhibitors of Multidrug Resistance Efflux Pumps in Pseudomonas Aeruginosa: Novel Agents for Combination Therapy. *Antimicrob. Agents Chemother.* **2001**, *45* (1), 105−116.

(21) Sharma, A.; Gupta, V. K.; Pathania, R. Efflux Pump Inhibitors for Bacterial Pathogens: From Bench to Bedside. *Indian J. Med. Res.* **2019**, *149* (2), 129−145.

(22) Turkson, N. Y. *MefA-Mediated Macrolide Resistance in Group A Streptococci: The Search for Efflux Pump Inhibitors from Marine Natural Products*, UC San Diego, 2021. https://escholarship.org/uc/item/3w09f4qh.

(23) Berbel, D.; González-Díaz, A.; López de Egea, G.; Càmara, J.; Ardanuy, C. An Overview of Macrolide Resistance in Streptococci: Prevalence, Mobile Elements and Dynamics. *Microorganisms* **2022**, *10* (12), 2316.

(24) Fostier, C. R.; Ousalem, F.; Leroy, E. C.; Ngo, S.; Soufari, H.; Innis, C. A.; Hashem, Y.; Boël, G. Regulation of the Macrolide Resistance ABC-F Translation Factor MsrD. *Nat. Commun.* **2023**, *14* (1), 3891.

(25) Varaldo, P. E.; Montanari, M. P.; Giovanetti, E. Genetic Elements Responsible for Erythromycin Resistance in Streptococci. *Antimicrob. Agents Chemother.* **2009**, *53* (2), 343−353.

(26) Ambroset, C.; Coluzzi, C.; Guédon, G.; Devignes, M.-D.; Loux, V.; Lacroix, T.; Payot, S.; Leblond-Bourget, N. New Insights into the Classification and Integration Specificity of Streptococcus Integrative Conjugative Elements through Extensive Genome Exploration. *Front. Microbiol.* **2016**, *6*, 1483.

(27) Iannelli, F.; Santoro, F.; Santagati, M.; Docquier, J.-D.; Lazzeri, E.; Pastore, G.; Cassone, M.; Oggioni, M. R.; Rossolini, G. M.; Stefani, S.; Pozzi, G. Type M Resistance to Macrolides Is Due to a Two-Gene Efflux Transport System of the ATP-Binding Cassette (ABC) Superfamily. *Front. Microbiol.* **2018**, *9*, 1670.

(28) Leclercq, R.; Courvalin, P. Resistance to Macrolides and Related Antibiotics in Streptococcus Pneumoniae. *Antimicrob. Agents Chemother.* **2002**, *46* (9), 2727−2734.

(29) Basu, S.; Naha, A.; Veeraraghavan, B.; Ramaiah, S.; Anbarasu, A. In Silico Structure Evaluation of BAG3 and Elucidating Its Association with Bacterial Infections through Protein−Protein and Host-pathogen Interaction Analysis. *J. Cell. Biochem.* **2021**, *123*, 115.

(30) Shankar, C.; Basu, S.; Lal, B.; Shanmugam, S.; Vasudevan, K.; Mathur, P.; Ramaiah, S.; Anbarasu, A.; Veeraraghavan, B. Aerobactin Seems To Be a Promising Marker Compared With Unstable RmpA2 for the Identification of Hypervirulent Carbapenem-Resistant Klebsiella Pneumoniae: In Silico and In Vitro Evidence. *Front. Cell. Infect. Microbiol.* **2021**, *11*, No. 709681.

(31) Varghese, R.; Basu, S.; Neeravi, A.; Pragasam, A.; Aravind, V.; Gupta, R.; Miraclin, A.; Ramaiah, S.; Anbarasu, A.; Veeraraghavan, B. Emergence of Meropenem Resistance Among Cefotaxime Non-

https://doi.org/10.1021/acsomega.3c05210
ACS Omega 2023, 8, 39454−39467

Susceptible Streptococcus Pneumoniae: Evidence and Challenges. *Front. Microbiol.* **2022**, *12*, 4111.
(32) Naha, A.; Ramaiah, S. Structural Chemistry and Molecular-Level Interactome Reveals Histidine Kinase EvgS to Subvert Both Antimicrobial Resistance and Virulence in Shigella Flexneri 2a Str. 301. *3 Biotech* **2022**, *12* (10), 258.
(33) Lemieux, M. J.; Huang, Y.; Wang, D. N. Crystal Structure and Mechanism of GlpT, the Glycerol-3-Phosphate Transporter from E. *Coli. Microscopy* **2005**, *54* (suppl_1), i43−i46.
(34) Basu, S.; Varghese, R.; Debroy, R.; Ramaiah, S.; Veeraraghavan, B.; Anbarasu, A. Non-Steroidal Anti-Inflammatory Drugs Ketorolac and Etodolac Can Augment the Treatment against Pneumococcal Meningitis by Targeting Penicillin-Binding Proteins. *Microb. Pathog.* **2022**, *170*, No. 105694.
(35) Debroy, R.; Ramaiah, S. Translational Protein RpsE as an Alternative Target for Novel Nucleoside Analogues to Treat MDR Enterobacter Cloacae ATCC 13047: Network Analysis and Molecular Dynamics Study. *World J. Microbiol. Biotechnol.* **2023**, *39* (7), 187.
(36) Garvey, M. I.; Piddock, L. J. V. The Efflux Pump Inhibitor Reserpine Selects Multidrug-Resistant Streptococcus Pneumoniae Strains That Overexpress the ABC Transporters PatA and PatB. *Antimicrob. Agents Chemother.* **2008**, *52* (5), 1677−1685.
(37) Shriram, V.; Khare, T.; Bhagwat, R.; Shukla, R.; Kumar, V. Inhibiting Bacterial Drug Efflux Pumps via Phyto-Therapeutics to Combat Threatening Antimicrobial Resistance. *Front. Microbiol.* **2018**, *9*, 2990.
(38) Abdel-Karim, S. A.-A. M.; El-Ganiny, A. M. A.; El-Sayed, M. A.; Abbas, H. A. A. Promising FDA-Approved Drugs with Efflux Pump Inhibitory Activities against Clinical Isolates of Staphylococcus Aureus. *PLoS One* **2022**, *17* (7), No. e0272417.
(39) Basu, S.; Naha, A.; Veeraraghavan, B.; Ramaiah, S.; Anbarasu, A. In Silico Structure Evaluation of BAG3 and Elucidating Its Association with Bacterial Infections through Protein−Protein and Host-pathogen Interaction Analysis. *J. Cell. Biochem.* **2022**, *123* (1), 115−127.
(40) Shankar, C.; Basu, S.; Lal, B.; Shanmugam, S.; Vasudevan, K.; Mathur, P.; Ramaiah, S.; Anbarasu, A.; Veeraraghavan, B. Aerobactin, Seems to Be a Promising Marker Compared to Unstable RmpA2 for the Identification of Hypervirulent Carbapenem-Resistant Klebsiella Pneumoniae: In-Silico and in-Vitro Evidence. *Front. Cell. Infect. Microbiol.* **2021**, *11*, 776.
(41) Schwede, T. SWISS-MODEL: An Automated Protein Homology-Modeling Server. *Nucleic Acids Res.* **2003**, *31* (13), 3381−3385.
(42) Webb, B.; Sali, A. Comparative Protein Structure Modeling Using MODELLER. *Curr. Protoc. Bioinform.* **2016**, *54* (1), 5−6.
(43) Heo, L.; Park, H.; Seok, C. GalaxyRefine: Protein Structure Refinement Driven by Side-Chain Repacking. *Nucleic Acids Res.* **2013**, *41* (Web Serverissue), 384−388.
(44) Kaplan, W.; Littlejohn, T. G. Swiss-PDB Viewer (Deep View). *Brief. Bioinform.* **2001**, *2* (2), 195−197.
(45) Naha, A.; Banerjee, S.; Debroy, R.; Basu, S.; Ashok, G.; Priyamvada, P.; Kumar, H.; Preethi, A. R.; Singh, H.; Anbarasu, A.; Ramaiah, S. Network Metrics, Structural Dynamics and Density Functional Theory Calculations Identified a Novel Ursodeoxycholic Acid Derivative against Therapeutic Target Parkin for Parkinson's Disease. *Comput. Struct. Biotechnol. J.* **2022**, *20*, 4271−4287.
(46) Gromiha, M. M.; Nagarajan, R.; Selvaraj, S. Protein Structural Bioinformatics: An Overview. In *Encyclopedia of Bioinformatics and Computational Biology: ABC of Bioinformatics*, Ranganathan, S.; Gribskov, M.; Nakai, K.; Schönbach, C., Eds.; Academic Press: Oxford, 2019; pp. 445−459.
(47) Wiltgen, M. Algorithms for Structure Comparison and Analysis: Homology Modelling of Proteins. In *Encyclopedia of Bioinformatics and Computational Biology: ABC of Bioinformatics*, Ranganathan, S.; Gribskov, M.; Nakai, K.; Schönbach, C., Eds.; Academic Press: Oxford, 2019; pp. 38−61.
(48) Geourjon, C.; Deléage, G. Sopma: Significant Improvements in Protein Secondary Structure Prediction by Consensus Prediction from Multiple Alignments. *Bioinformatics* **1995**, *11* (6), 681−684.
(49) Lomize, M. A.; Pogozheva, I. D.; Joo, H.; Mosberg, H. I.; Lomize, A. L. OPM Database and PPM Web Server: Resources for Positioning of Proteins in Membranes. *Nucleic Acids Res.* **2012**, *40* (Database issue), D370−D376.
(50) Van Der Spoel, D.; Lindahl, E.; Hess, B.; Groenhof, G.; Mark, A. E.; Berendsen, H. J. C. GROMACS: Fast, Flexible, and Free. *J. Comput. Chem.* **2005**, *26* (16), 1701−1718.
(51) Lemkul, J. From Proteins to Perturbed Hamiltonians: A Suite of Tutorials for the GROMACS-2018 Molecular Simulation Package [Article v1.0]. *Living J. Comput. Mol. Sci.* **2019**, *1* (1), 1−53.
(52) Miryala, S. K.; Basu, S.; Naha, A.; Debroy, R.; Ramaiah, S.; Anbarasu, A.; Natarajan, S. Identification of Bioactive Natural Compounds as Efficient Inhibitors against Mycobacterium Tuberculosis Protein-Targets: A Molecular Docking and Molecular Dynamics Simulation Study. *J. Mol. Liq.* **2021**, *341*, No. 117340.
(53) Rossos, G.; Hadjikakou, S. K.; Kourkoumelis, N. Molecular Dynamics Simulation of 2-Benzimidazolyl-Urea with DPPC Lipid Membrane and Comparison with a Copper(II) Complex Derivative. *Membranes* **2021**, *11* (10), 743.
(54) Wallace, A. C.; Laskowski, R. A.; Thornton, J. M. LIGPLOT: A Program to Generate Schematic Diagrams of Protein-Ligand Interactions. *Protein Eng. Des. Sel.* **1995**, *8* (2), 127−134.
(55) Pettersen, E. F.; Goddard, T. D.; Huang, C. C.; Couch, G. S.; Greenblatt, D. M.; Meng, E. C.; Ferrin, T. E. UCSF Chimera-A Visualization System for Exploratory Research and Analysis. *J. Comput. Chem.* **2004**, *25* (13), 1605−1612.
(56) Jamroz, M.; Kolinski, A.; Kmiecik, S. CABS-Flex: Server for Fast Simulation of Protein Structure Fluctuations. *Nucleic Acids Res.* **2013**, *41* (1), 427−431.
(57) Morris, G. M.; Huey, R.; Lindstrom, W.; Sanner, M. F.; Belew, R. K.; Goodsell, D. S.; Olson, A. J. AutoDock4 and AutoDockTools4: Automated Docking with Selective Receptor Flexibility. *J. Comput. Chem.* **2009**, *30* (16), 2785−2791.
(58) Jejurikar, B. L.; Rohane, S. H. Drug Designing in Discovery Studio. *Asian J. Res. Chem.* **2021**, *14* (2), 135−138.
(59) Naha, A.; Vijayakumar, S.; Lal, B.; Shankar, B. A. Genome Sequencing and Molecular Characterisation of XDR Acinetobacter Baumannii Reveal Complexities in Resistance: Novel Combination of Sulbactam-Durlobactam Holds Promise for Therapeutic Intervention. *J. Cell. Biochem.* **2021**, *122*, 1946−1957.
(60) Basu, S.; Veeraraghavan, B.; Ramaiah, S.; Anbarasu, A. Novel Cyclohexanone Compound as a Potential Ligand against SARS-CoV-2 Main-Protease. *Microb. Pathog.* **2020**, *149*, No. 104546.
(61) Vasudevan, K.; Basu, S.; Arumugam, A.; Naha, A.; Ramaiah, S.; Anbarasu, A.; Veeraraghavan, B. Identification of Potential Carboxylic Acid-Containing Drug Candidate to Design Novel Competitive NDM Inhibitors: An in-Silico Approach Comprising Combined Virtual Screening and Molecular Dynamics Simulation. *bioRxiv* **2021**, DOI: 10.1101/2021.07.05.451101.

https://doi.org/10.1021/acsomega.3c05210
ACS Omega 2023, 8, 39454−39467